

Evaluation of nanoparticles for nanoscale film fabrication harnessing tribochemistry

Yuyang Yuan^{a,*}, Chun Wang^a, Seunghwan Lee^a, Mark C.T. Wilson^b, Ardian Morina^a

^a Institute of Functional Surface, School of Mechanical Engineering, University of Leeds, Woodhouse Lane, Leeds LS2 9JT, UK

^b Institute of Thermofluids, School of Mechanical Engineering, University of Leeds, Woodhouse Lane, Leeds LS2 9JT, UK

ARTICLE INFO

Keywords:

Tribofilms
Lubricant additives
Thin film fabrication

ABSTRACT

Tribofilms, essential for reducing friction and wear in mechanical systems, are typically formed on contact surfaces through tribochemical reactions during sliding or rolling interactions. Nanofabrication of zinc dialkyl dithiophosphate (ZDDP) tribofilm provides an alternative manufacturing technique for developing micro/nano-scale structures and devices for applications other than reducing friction and wear. While ZDDP tribofilms can be fabricated with nanometer-level precision, the application of this tribologically fabricated thin film was limited by its electrically insulating nature. Nanoparticles, with their unique thermal, electrical, and optical properties, offer the potential to enhance the capabilities of fabricated tribofilms. This study investigates the role of five nanoparticles—WS₂, Al₂O₃, CuO, BN, and TiO₂—in the fabrication of tribofilms on a steel substrate. The thickness, distribution, and composition of the fabricated tribofilms were analysed. To accurately characterise the distribution and thickness of tribofilms, an innovative methodology utilising Conductive Atomic Force Microscopy (CAFM) has been developed. The results reveal that while the addition of WS₂, Al₂O₃, and CuO do not affect the tribofilm composition compared with pure base oil, BN and TiO₂ are chemically incorporated into the tribofilm, altering its composition and potentially enhancing its functional properties.

1. Introduction

Tribofilms are thin layers of material that form on surfaces as a result of mechanical and chemical interactions during tribological processes, often involving tribochemical reactions between the surface and lubricants [1]. These films play a crucial role in reducing friction by creating a low shear strength layer between surfaces or acting as a protective barrier that minimises direct contact, thereby decreasing wear. Zinc dialkyl dithiophosphate (ZDDP) is an effective lubricant additive that forms robust phosphate glass-based tribofilms [2,3], mitigating wear while also providing anti-corrosion benefits. The formation of ZDDP tribofilms is driven by stress, with tribochemical reactions occurring at the asperities of the interacting surfaces in direct solid contact [4]. Recent works also revealed that stress can be applied via shear forces [5], where the asperities of the interacting surfaces are not in direct solid contact with each other. Both shear stress and elevated temperature promote tribofilm growth through stress-augmented thermal activation [6]. Therefore, by controlling contact parameters such as load, sliding speed, and temperature, the growth of tribofilms can be effectively adjusted [4,7].

In the semiconductor, integrated circuit (IC), and micro-electromechanical system (MEMS) device manufacturing industries, nanofabrication is crucial for developing micro/nano-scale structures and devices with electronic, thermal, and optical properties. Current nanolithography techniques include methods such as photolithography [8] and nanoimprint lithography [9], which transfer patterns from moulds. Other methods, like electron beam lithography (EBL) [10] and scanning probe lithography (SPL) [11], can fabricate patterns through direct writing or scanning without the need for templates or masks, making the manufacturing process more flexible. However, none of the above mentioned techniques can simultaneously satisfy all the needs as nanotechnology continues to develop towards diversification and depth [12].

To implement tribochemistry beyond typical tribological applications, the fabrication of thin films utilising tribochemistry provides an alternative manufacturing technique that can create these films in situ during the tribological process. By leveraging insights from ZDDP tribochemistry, the generation of tribofilms presents a novel approach for thin film fabrication [13,14]. Immersing an AFM tip in lubricant, tribochemical reactions are induced between the AFM probe and the

* Corresponding author.

E-mail address: mnyyu@leeds.ac.uk (Y. Yuan).

<https://doi.org/10.1016/j.triboint.2025.110805>

Received 21 December 2024; Received in revised form 5 May 2025; Accepted 13 May 2025

Available online 14 May 2025

0301-679X/© 2025 The Authors. Published by Elsevier Ltd. This is an open access article under the CC BY-NC license (<http://creativecommons.org/licenses/by-nc/4.0/>).

substrate, facilitating highly controllable and precise tribofilm growth [4,7,13–15]. Using this method, the ZDDP tribofilms can achieve lateral dimensions as fine as 100 nm and vertical resolutions of 10 nm. This newly developed manufacturing technique provides a versatile and controllable method to produce nanoscale 3D architectures with a simple fabrication process, making it particularly valuable for expanding fields such as flexible electronics and sensor technologies [13,16]. Furthermore, another study demonstrated that composite structures can be generated by sequentially layering films of zirconia and ZDDP [14], which may enhance the mechanical and thermal properties, thereby highlighting the potential for developing complex, multifunctional tribofilms.

However, despite their advantageous mechanical properties in reducing wear, ZDDP tribofilms are electrically insulating [17], which limits their potential application in high-precision fabrication for electronic devices. Beyond ZDDP, nanoparticles have also been utilised as additives in lubricants to effectively reduce wear and decrease friction via surface deposition and tribofilm formation [18–22]. The formation of the tribofilm can be explained by tribochemical reactions between nanoparticles and the substrate due to the high pressure and flash temperature generated by the contact of asperities during the tribological process [23,24]. Another mechanism for explaining film formation involves triboinsertion, particularly with metal oxide nanoparticles [15, 25,26]. The entry of nanoparticles into the contact area between surfaces is crucial for generating the tribofilm. However, due to the difficulty in identifying the movement of nanoparticles during the tribological process, the fundamental interactions leading to tribofilm formation are not completely understood.

In additive manufacturing, nanoparticles have also been developed to assemble at specific positions, leveraging their unique mechanical, electrical, thermal, and optical properties [27]. Nanoparticles like WS₂, Al₂O₃, CuO, BN, and TiO₂ show promise in additive manufacturing, particularly in applications such as circuit and sensor fabrication, where they can enhance material properties and functionality [28–32]. These nanoparticles have also been used in tribological research for their ability to reduce friction and protect surfaces through tribofilm formation [18,20,21,33,34]. Fabricating the tribofilm with these nanoparticles offers possible functionalities beyond merely reducing wear and friction. However, previous research in tribology has primarily focused on the applications of these materials in wear and friction reduction, indicating a gap in understanding their multifunctional capabilities and potential usage in thin film fabrication harnessing the tribochemical reaction during the tribology process.

From the perspective of thin film fabrication, the thickness, surface distribution, composition, and interactions during the film formation process require further analysis to optimise the performance and functionality of tribofilms generated from nanoparticles. As the application scenarios differ, nanoparticles used in tribology research are typically blended into various base oils containing different dispersants and additives, and are tested under a wide range of contact conditions. To ensure that the same films are formed under specific conditions and with particular nanoparticles, it is crucial to develop a method that can characterise the tribofilms generated on the substrate and provide insights into the mechanisms by which the films are formed.

This study selected five types of nanoparticles—WS₂, Al₂O₃, CuO, BN, and TiO₂—to investigate their potential for fabricating thin films by harnessing tribochemistry. As this research associates tribology in a positive way to fabricate thin films, it primarily emphasises examining the thickness, surface distribution, and structural composition of the generated tribofilms, which are crucial for optimising their performance in various applications. To address the challenges in tribofilm thickness characterisation, a method based on Conductive-AFM has been developed. These findings aim to provide a foundational reference for further utilisation of these nanoparticles in the fabrication of nanostructures.

2. Materials and methods

2.1. Materials

The steel plate (EN31, 7 × 7 × 3 mm dimensions, 57.8 ± 1.02 nm roughness) was selected as the substrate for the tribofilm deposition, a steel pin (EN31, 10 mm radius, 401.6 ± 1.2 nm roughness) was selected as the upper part of the friction pair. Synthetic PAO base oil (Synfluid PAO 8 cSt) was used as the carrier for nanoparticles and control group for comparison. Other carrier solvents will be considered in future work, specifically tailored to different applications. EN31 Steel and PAO base oil are commonly used in tribological studies, making it easier to compare results with existing literature and validate test results across different studies.

Al₂O₃, BN, CuO, TiO and WS₂ were purchased from Sigma-Aldrich, details of the nanoparticles provided by the supplier were presented in Table 1. Nanoparticles were ultrasonically dispersed into the PAO base oil at 0.2 wt%, in line with the effective concentration in the previous investigations [18,20–22,35]. To clarify the performance of these nanoparticles in tribofilm generation, no chemical modification was made to these nanoparticles to improve their dispersion ability in oil. After the ultrasonication process, all nanoparticles could be dispersed well, however, they were inclined to precipitate several hours later. Therefore, before each tribofilm fabrication test, the tested mixture of oil and nanoparticle was ultrasonicated for 1 hour to ensure the nanoparticles dispersed homogeneously within the oil with the naked eye [36].

2.2. Tribofilm fabrication

Tribofilm fabrication tests were carried out using UMT Tribolab, Bruker. Test details can be found in Table 2. Maximum contact pressure in the tests was 1.6 GPa based on Hertzian contact theory to ensure the working condition under the boundary lubrication regime (Lambda ratio < 1) calculated using Hamrock-Dowson equation. All experiments were carried out three times to ensure repeatability. Before each test, plates and pins were cleaned with acetone for 20 min in an ultrasonic bath. After the experiment, samples were cleaned using heptane to remove the remaining oil on the substrate. Before each tribofilm fabrication test, the tested mixture of oil and nanoparticle was ultrasonicated for 1 hour to ensure the nanoparticles dispersed homogeneously within the oil with the naked eye [36].

2.3. Tribofilm analysis

2.3.1. Tribofilm thickness

In previous research, tribofilm thickness is commonly determined using vertical cross-section analysis along several selected lines from morphology images obtained in AFM contact, tapping mode or peak force tapping mode. In this study, conductive-AFM was employed to simultaneously obtain force, current, and height information, allowing for precise measurement of the tribofilm profile on the substrate. With conductive-AFM, the force curve and current data can be recorded simultaneously, as shown in Fig. 1. As the AFM tip approaches the substrate surface, a force signal is detected when the tip contacts the

Table 1
Nanoparticles for tribofilm fabrication (particle size details as provided by supplier).

Material	Description
Tungsten (IV) sulfide	90 nm avg. particle size (SEM)
Boron nitride	< 150 nm avg. particle size (TEM)
Titanium (IV) oxide	< 25 nm particle size
Copper (II) oxide	< 50 nm particle size (TEM)
Aluminum oxide	30–60 nm particle size (TEM)

Table 2
Tribofilm fabrication test conditions.

Load	Temperature	Duration	Speed
160 N	Room temperature	2 h	0.1 m/s (5 mm stroke at 10 Hz)

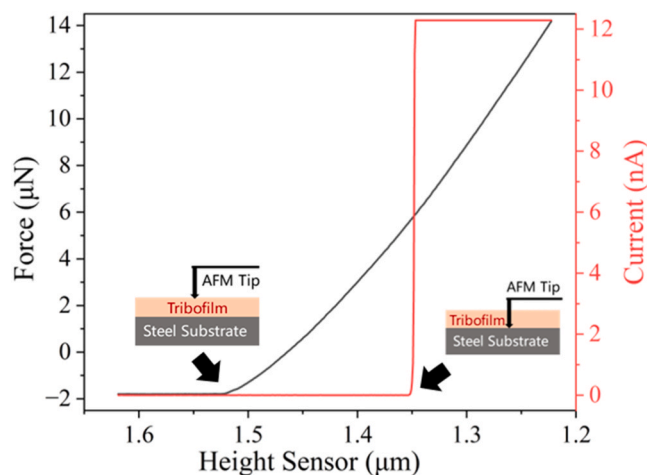


Fig. 1. Single point force curve mapping data of force and current obtained with C-AFM.

substrate, indicating the upper surface of the tribofilm. At this point, no current signal is detected because the tribofilm is non-conductive. As the tip penetrates the tribofilm and approaches the steel substrate, a current signal is detected, marking the bottom surface of the tribofilm layer. By combining the height information at the points where the force and current signals are detected, the tribofilm thickness can be calculated.

By repeatedly performing force curve mapping within the scanned area, the thickness and distribution of the tribofilm can be obtained (Fig. S1 in Supplementary information shows different force curves in a mapping area to obtain the tribofilm thickness). A conductivity accessory coupled with Dimension Icon AFM (Bruker) was used to characterise the morphology and electronic properties of the films under ambient conditions. Wear-resistant diamond tips with a 200 N/m cantilever spring constant (NM-TC, Adama Innovations Ltd.) were employed in conductive-AFM mode, where a bias was applied to the sample. The maps were taken from a $5 \times 5 \mu\text{m}^2$ area in the centre of the fabricated tribofilm, consisting of 60×60 individual force curve data points. For each type of tested tribofilm, three mapping analyses were conducted at different locations. To verify the reliability of this measurement method, the tribofilm thickness obtained by the C-AFM method was compared with results obtained by FIB/TEM and will be discussed in the results and discussion part.

The steel plate surface worn area will also be analysed with a white light interferometry (NPFLEX, Bruker) to evaluate the influence of this tribological thin film fabrication process after the tests.

2.3.2. Tribofilm characterisation

To analyse the composition of the fabricated tribofilm on the substrate, static Secondary-Ion Mass Spectrometry (SIMS) measurements were performed using a Hiden Compact SIMS, equipped with a MAXIM-600P detector. This detector features a Hiden 6 mm triple quadrupole mass filter and pulse ion detection capabilities. An Ar^+ primary ion beam with an ion energy of 5000 V and an emission current of $10.0 \mu\text{A}$ was used to measure the mass-to-charge (m/z) range between 1 and 300. The sample area for both positive and negative spectra was $500 \times 500 \mu\text{m}^2$.

A confocal Raman spectrometer (InVia, Renishaw) was used to detect

the chemical species of the fabricated tribofilm ($1 \mu\text{m} \times 1 \mu\text{m}$). The Raman spectra were obtained in the wavenumber range of $1650\text{--}150 \text{ cm}^{-1}$ with a laser excitation of 488 nm at 10 % laser power and 10 s exposure time. The laser power and exposure time were selected to ensure signal intensity while not damaging the tribofilm on the surface.

To investigate the tribofilm physical structure and composition, cross-sections were prepared using a high-resolution Focused Ion Beam (FIB, Helios G4 CX DualBeam). The surfaces were transversely cut with FIB to fabricate cross-sectional lamellar specimens. A chromium (Cr) layer was deposited on the sample to make it conductive and to protect the sample from damage by the electron and ion beams. Subsequently, a platinum (Pt) layer was deposited to further protect the sample from the ion beam during milling to create the lamellar for TEM analysis. The prepared cross-sectional lamellar were analysed using an FEI Titan3 Themis 300 Scanning Transmission Electron Microscope (STEM) equipped with a Gatan Quantum ER energy filter, Energy Dispersive X-ray (EDX), and High-Angle Annular Dark-Field Scanning (HAADF) detectors.

3. Results and discussion

3.1. Tribology tests and tribofilm thickness

Fig. 2a shows the coefficients of friction and film thickness after tribology tests with the tested nanoparticles and PAO base oil. The results indicate that the addition of 0.2 wt% additives led to variations in both friction and tribofilm thickness compared to the PAO base oil. Al_2O_3 , BN and WS_2 nanoparticles demonstrated a reduction in friction, which is consistent with previous reports [20,21,23]. However, TiO_2 and CuO exhibited slightly increased friction compared to the base oil, a trend that has also been observed in [37,38]. Given that the test conditions and nanoparticle parameters (such as size, concentration, and surface modification) differ from those in prior studies, it can be suggested that the friction performance is significantly affected by the testing conditions, even though all tests were nominally conducted in the boundary lubrication regime.

As shown in Fig. 2a, without any additive, the PAO base oil resulted in an average tribofilm of 24 nm thick on the substrate. This tribofilm may have originated from the dissociation of C–C and C–H bonds in the linear olefins of the PAO base oil [39]. The error bar shows that the film thickness varies at different measurement points, which may be related to the weak bonding of the PAO tribofilm to the substrate [40]. Compared to the results with PAO base oil, CuO produced a greater film thickness, although there was considerable variation in thickness across different regions. The increase in tribofilm thickness might be related to the catalytic effect of Cu as a transition metal on the carbon-based tribofilm [41] or to the formation of the tribofilm from CuO particles themselves [42]. Al_2O_3 , TiO_2 , and WS_2 additives could also generate tribofilm on the substrate, the film thickness was similar to the PAO base oil. The addition of BN also resulted in an increase in tribofilm thickness and demonstrated better consistency across different test areas. Interestingly, when correlating these findings with the corresponding friction results, there does not appear to be a clear relationship between tribofilm thickness and the coefficient of friction. As the PAO base oil formed a tribofilm on the substrate, it is necessary to confirm whether the tribofilm can also be fabricated with nanoparticles based on further chemical analysis.

Although the aim of this work is to study the tribofilm formation and not specifically the anti-wear performance, it is of interest to report the wear of the substrate especially to facilitate a better understanding of tribofilm formation. From Fig. 2b, it can be observed that the substrate experiences wear when using PAO base oil along with BN, CuO, and WS_2 nanoparticles. In contrast, TiO_2 and Al_2O_3 nanoparticles could reduce substrate wear during the film fabrication process. The wear reduction effect of TiO_2 and Al_2O_3 nanoparticles correlates well with previous

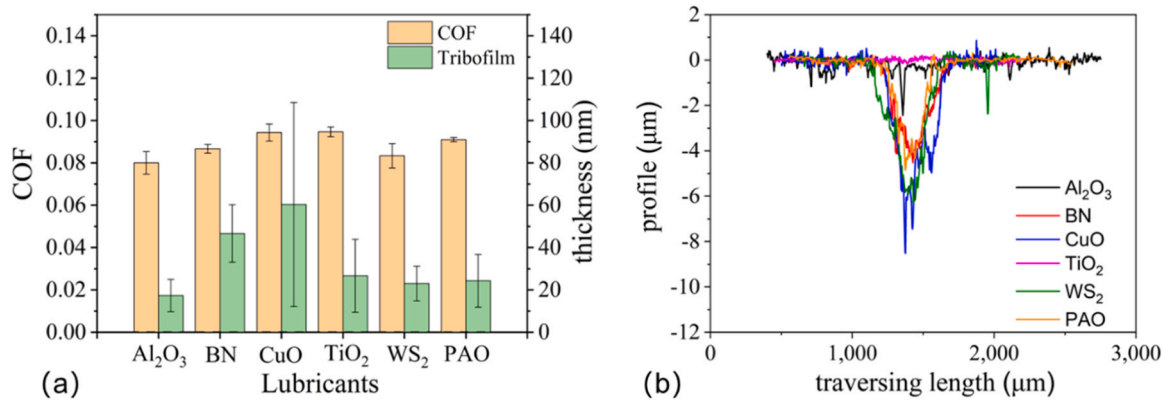


Fig. 2. (a) COF and tribofilm thickness of nanoparticles and PAO base oil, (b) Cross-sectional profiles of the steel plate wear track after tests. The coefficient of friction (COF) value was calculated by averaging the last five minutes of data, as the friction reached a relatively steady state. The COF and tribofilm data presented are the averages of three repeated measurements (Fig. S2 in [Supplementary information](#)) and the error bars represent the standard deviation.

work. The addition of BN, CuO, and WS₂ has also been reported to have a wear reduction effect before; however, the discrepancy here may be caused by differences in working conditions and nanoparticle parameters.

3.2. Surface morphology and tribofilm distribution

Fig. 3 illustrates the AFM height images and the corresponding 3D film thickness maps for various nanoparticle additives and PAO base oil. The substrate morphology varies significantly with different additives, making it challenging to accurately determine the tribofilm thickness and distribution based solely on AFM height images. However, using the C-AFM method mentioned in the previous section, the tribofilm thickness and distribution on the substrate could be obtained. For the PAO base oil, the tribofilm generated appears to have the ridge-like pattern with a non-uniform distribution. The Al₂O₃ and WS₂ nanoparticles produce tribofilms similar to those formed by the PAO base oil, also indicating non-uniform coverage.

Fig. 3 shows that BN nanoparticles form a tribofilm with a larger surface area coverage and greater thickness than PAO, but its distribution is characterised by peak-like protrusions rather than uniform surface coverage. The tribofilm formed with TiO₂ nanoparticles exhibits a relatively uniform and consistent distribution; however, this uniform coverage is observed over only about half of the tested area. In contrast, the tribofilm generated by CuO nanoparticles provides the most comprehensive surface coverage and the highest average thickness among the tested additives. However, the thickness of the tribofilm still varies across different regions, and its surface is notably uneven.

Since the tribofilm in this study aims to be considered as the fabricated thin film, statistical data on its thickness will be further emphasised. The tribofilm thickness data obtained through C-AFM were plotted as histograms in **Fig. 4** to better analyse the thickness distribution of the fabricated tribofilms. The histograms reveal that, for the PAO base oil, the majority of the tribofilm thickness is only a few nanometres across most areas, with some regions exhibiting coverage in the tens of nanometres. The tribofilm thickness distributions for Al₂O₃ and WS₂ nanoparticles show similarities to that of the PAO base oil, with a higher concentration of data points in the lower height regions, indicating uneven tribofilm coverage. In contrast, the TiO₂ tribofilm exhibits a greater number of data points within the higher thickness range of 50–150 nm, indicating the formation of a relatively uniform tribofilm over certain surface areas. However, the significant number of data points in the lower thickness range also suggests that the tribofilm does not achieve complete coverage across the entire surface.

The data for the BN tribofilm from **Fig. 4** reveal a substantial number of data points in the 150–200 nm range, as well as a significant number

of data points below 25 nm, supporting the observation from AFM images that the surface morphology of this tribofilm is characterised by peak-like protrusions rather than a uniform layer. In contrast, the CuO tribofilm exhibits a data point distribution that does not decrease steadily with increasing thickness; instead, clusters are observed around the 50 nm and 150 nm marks, suggesting variability in thickness across the film. This pattern indicates that the CuO tribofilm possesses the greatest average thickness among the tested additives and demonstrates surface undulations resulting from the uneven distribution of thickness.

3.3. Chemical structure of the tribofilm

3.3.1. SIMS

As illustrated in **Fig. 5**, the positive mass spectra for the tribofilm generated from PAO base oil reveal several peaks attributed to hydrocarbon fragments, specifically C₂H₇⁺ and C₆H₇⁺, along with iron species (Fe⁺). These findings suggest that the tribofilm consists of both organic components and metallic elements, likely originating from the base oil and the interacting surfaces. Similarly, the tribofilms formed in the presence of Al₂O₃, WS₂, and CuO nanoparticles exhibit positive mass spectra comparable to these of the PAO base oil tribofilm. These spectra contain peaks corresponding to hydrocarbon fragments and iron species, yet no signals related to the nanoparticle elements themselves were detected. This suggests that while these nanoparticles influence the formation of the tribofilm, they do not significantly incorporate their own elemental components into the tribofilm structure. Instead, the films are primarily composed of hydrocarbons and iron, suggesting that the nanoparticles are not involved in the tribochemical processes necessary for forming the film.

For the TiO₂ nanoparticles, the positive mass spectra exhibit intense signals for titanium species, specifically Ti⁺ and TiO⁺, indicating the presence of titanium elements within the tribofilm. This suggests that the TiO₂ nanoparticles not only influence the formation of the tribofilm but are also incorporated into its structure, contributing to its properties. In the case of BN nanoparticles, the detection of a B⁺ signal in the positive mass spectra confirms the presence of boron within the film, suggesting that the BN nanoparticles are partially integrated into the tribofilm. For negative mass spectra (**Fig. 6**), the tribofilm generated from PAO base oil exhibits characteristic carbon and oxygen fragments, specifically C⁻, C₂⁻, and O⁻. This indicates the presence of carbonaceous and oxidised components within the tribofilm. For the Al₂O₃, TiO₂, and WS₂ additives, the mass spectra similarly reveal no signals corresponding to their respective elements, with only carbon and oxygen fragments detected. For CuO, the detected C₆⁻ and C₄H₈O₂⁻ indicate that under the catalytic action of Cu, PAO will undergo degradation to form lubricating hydrocarbon compounds [43] and therefore the highest thickness

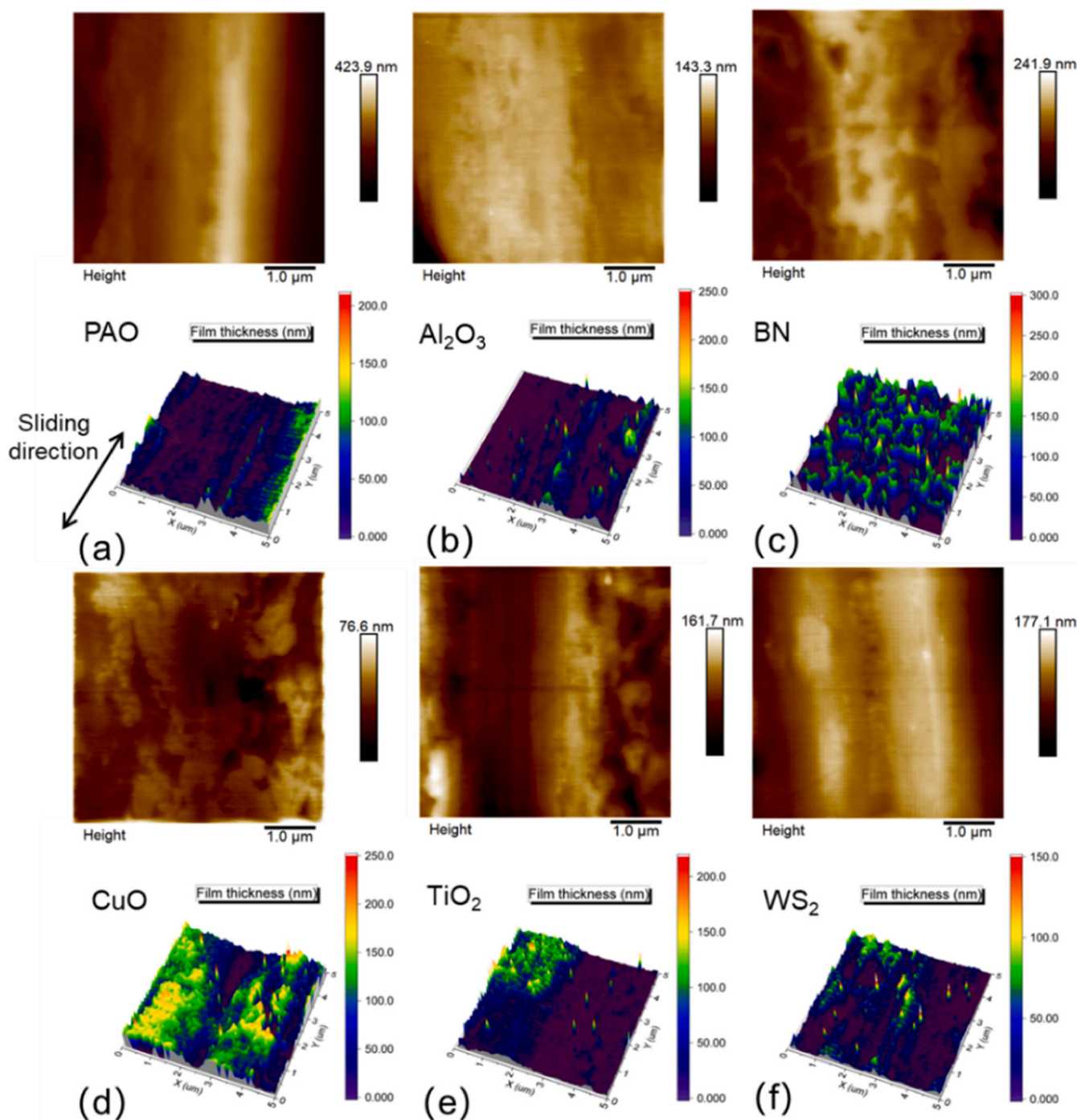


Fig. 3. AFM topography and C-AFM tribofilm images of (a) PAO, (b) Al₂O₃, (c) BN, (d) CuO, (e) TiO₂ and (f) WS₂ (Topographic and C-AFM images were obtained by analysing at least three different locations within the wear scar, Fig. S3 and Fig. S4 in Supplementary information).

tribofilm detected in previous tests.

The mass spectra of the tribofilm formed with BN additives display a series of peaks attributable to boron-containing fragments, specifically BO⁻ and BO₂⁻. This clearly demonstrates the presence of boron within the tribofilm, indicating that the BN nanoparticles are partially incorporated into the tribofilm structure. However, the absence of BN⁺ or BN⁻ signal in both positive and negative mass spectra suggests that the BN nanoparticles do not remain in their original structure within the film. Depth profiling data (Fig. S5a, b) reveal that the BO₂⁻ signal extends to a depth of about 45 nm, and the BO⁻ signal reaches about 82.5 nm. Considering the average tribofilm thickness of 55 nm obtained from C-AFM measurements, this implies that within the film formed by BN

additives, boron exists primarily in the form of boron oxides. The detection of these boron oxide species indicates that BN contributes to the chemical composition of the tribofilm via tribochemical reactions.

3.3.2. Raman

As shown in Fig. 7, Raman spectroscopy analysis of the tribofilms reveals distinct peaks corresponding to various chemical compositions within the tribofilms generated from PAO base oil and nanoparticle additives. For the PAO base oil, the Raman peaks observed around 226 cm⁻¹, 300 cm⁻¹, 412 cm⁻¹, and 1322 cm⁻¹ are characteristic of hematite (Fe₂O₃) [44], while the peak at approximately 668 cm⁻¹ indicates the presence of magnetite (Fe₃O₄) [45]. Additionally,

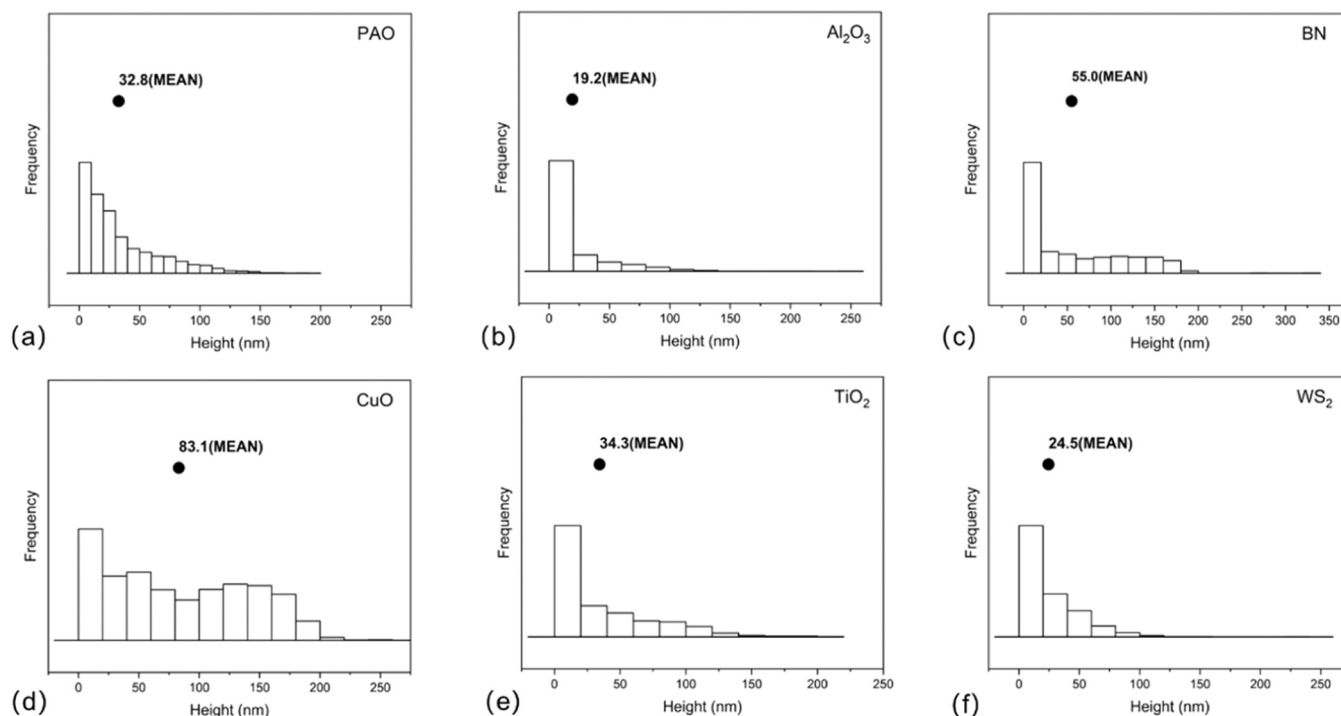


Fig. 4. Histograms of tribofilm profile data of (a) PAO, (b) Al₂O₃, (c) BN, (d) CuO, (e) TiO₂ and (f) WS₂.

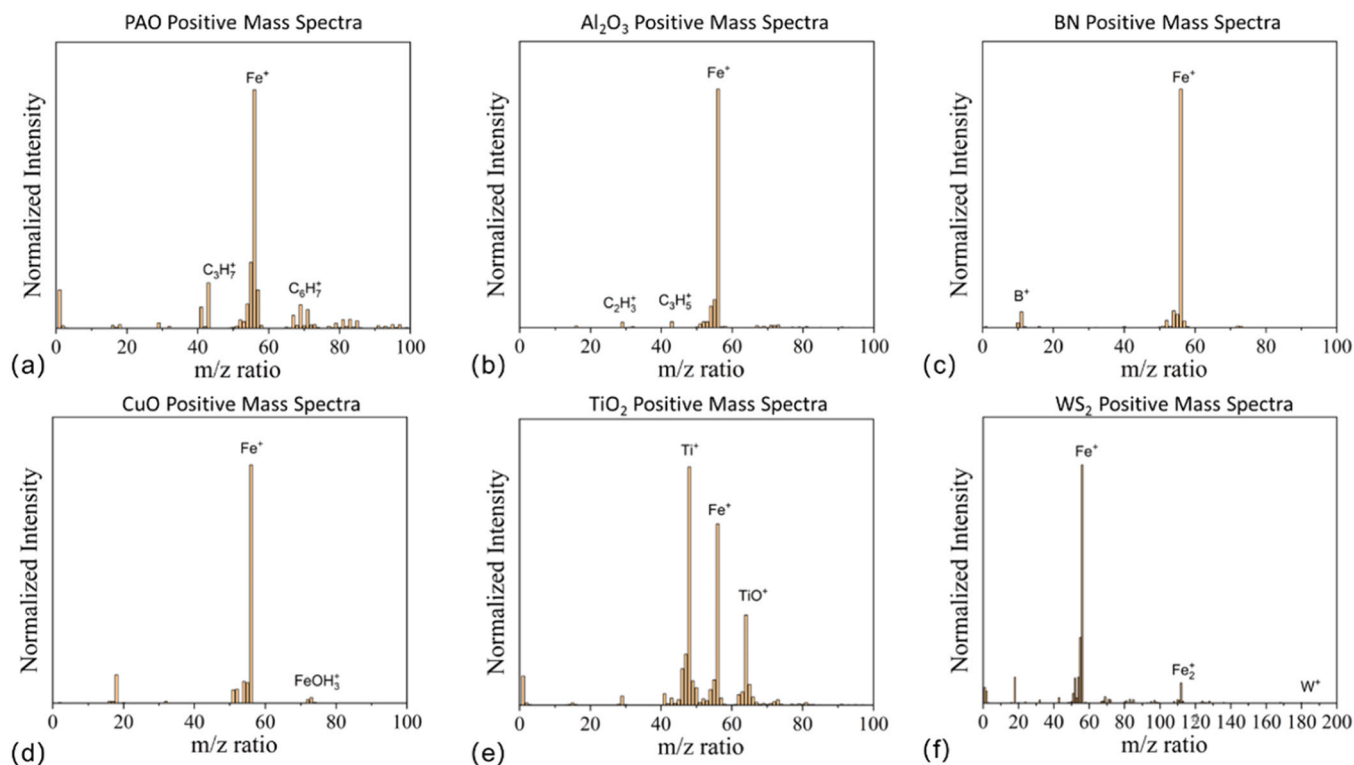


Fig. 5. SIMS positive mass spectra of (a) PAO, (b) Al₂O₃, (c) BN, (d) CuO, (e) TiO₂ and (f) WS₂.

a peak at 1590 cm⁻¹ is attributed to carbon [46], suggesting the presence of carbonaceous material within the tribofilm. Raman spectra for the Al₂O₃, CuO, and WS₂ additives indicated the presence of hematite, magnetite, and carbon within the tribofilms, with no significant incorporation of elements from the nanoparticles themselves, which confirms the observation from SIMS results. This suggests that these three types of

nanoparticles do not embed within the tribofilm structure but may only influence the formation of iron oxide and carbon-rich films on the substrate. For BN, a peak at 1366 cm⁻¹ [18] could be observed inside tribofilm. Unlike the sharp peak seen in pure BN nanoparticles, the broader peak detected in tribofilm suggests structural modification, likely influenced by the presence of boron oxide [47] formed during the

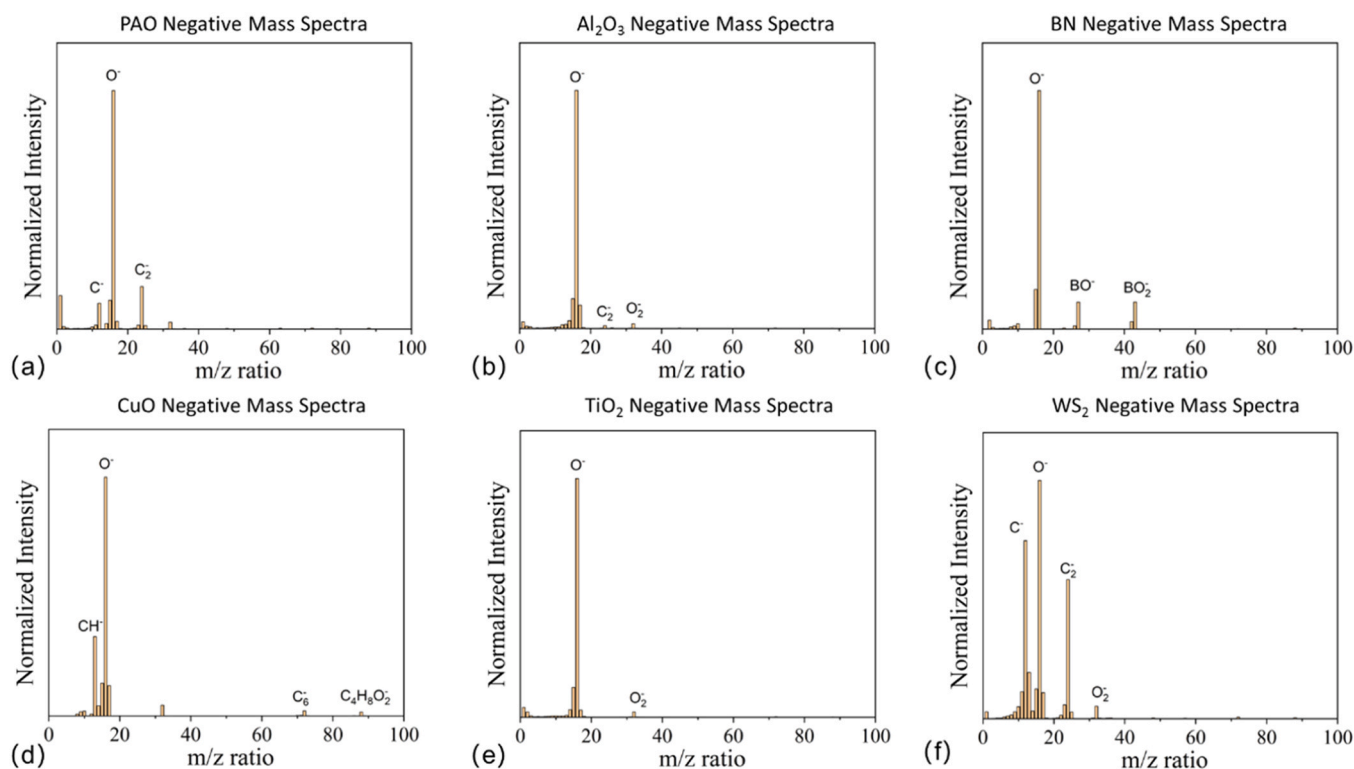


Fig. 6. SIMS negative mass spectra of a) PAO, b) Al_2O_3 , c) BN, d) CuO, e) TiO_2 and f) WS_2 .

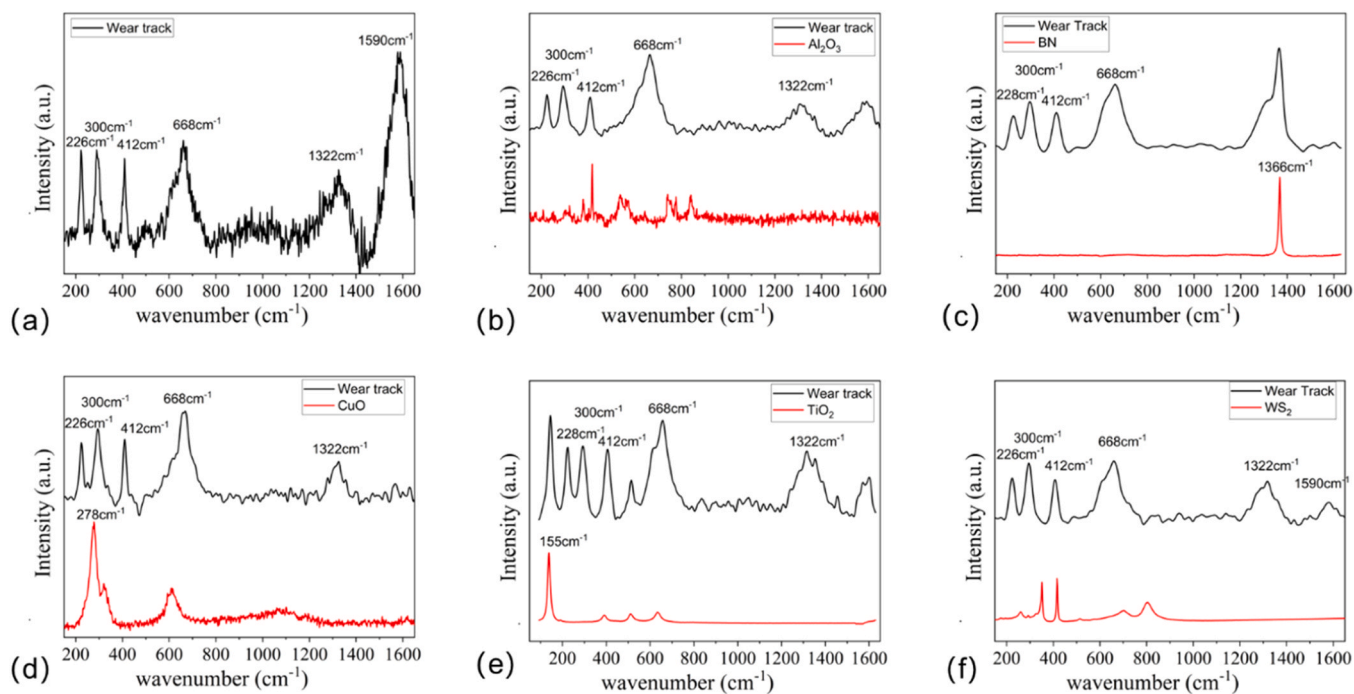


Fig. 7. Raman spectra of (a) PAO, (b) Al_2O_3 , (c) BN, (d) CuO, (e) TiO_2 and (f) WS_2 .

tribochemical process. The tribofilm of TiO_2 revealed an intense peak of around 155 cm^{-1} [22], confirming the presence of titanium oxide within the tribofilm structure.

3.3.3. TEM

To further elucidate the structure of the tribofilms formed on the surface, cross section samples prepared by FIB processing were analysed

using TEM. Since the previous analysis revealed that only BN and TiO_2 were incorporated into the tribofilm, the PAO, BN, and TiO_2 samples will be compared in subsequent studies. The PAO base oil sample (Fig. 8a) exhibits a distinct two-layered tribofilm, with an uneven thickness ranging from approximately 50 to 100 nm. Although the measurement cannot be guaranteed to be in the exact same area, the thickness and uneven distribution of the tribofilm here show good consistency with the

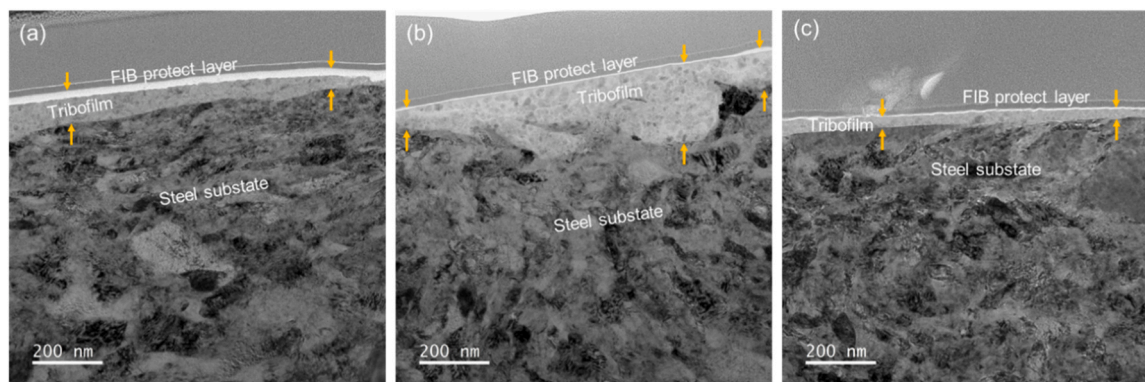


Fig. 8. TEM images of (a) PAO, (b) BN and (c) TiO₂ tribofilm.

results obtained by C-AFM. In contrast, the C-AFM method provides a broader view of tribofilm distribution and three-dimensional height information. The analysis area could be selected more easily as the complex FIB process to prepare the TEM sample will not be needed. This further avoids potential alterations to the tribofilm morphology caused by coating and ion beam processing during TEM sample preparation.

The tribofilm generated with BN nanoparticles (Fig. 8b) is accompanied by significant plastic deformation of the steel substrate. This severe deformation likely accounts for the peak-like protrusions observed in the tribofilm profile using the C-AFM method, where the tribofilm exhibits a non-uniform distribution rather than a smooth, even layer. In contrast, the tribofilm formed in the presence of TiO₂ nanoparticles displays a clear interface between the tribofilm and the steel substrate (Fig. 8c). Remarkably, the plastic deformation of the steel substrate appears to be mitigated, allowing the tribofilm to distribute more uniformly across the flattened surface. This suggests that the incorporation of TiO₂ nanoparticles not only contributes to the formation of the tribofilm but also helps in restoring the substrate's surface integrity, leading to a more even and consistent tribofilm distribution.

Further analysis of the tribofilm generated from PAO (Fig. 9) reveals a two-layer structure: the upper layer, approximately 10–20 nm thick, is primarily amorphous carbon, while the lower layer is composed of iron oxides. During the tribological process, the linear olefins in PAO undergo dehydrogenation [39], leading to the formation of a carbon-based solid-lubricating tribofilm [41,48]. Simultaneously, the iron oxide wear debris generated during friction increases the dissociation rate of C–C and C–H bonds, facilitating the formation of the two-layer tribofilm structure [49].

Observation of the tribofilm formed with BN nanoparticles, as shown

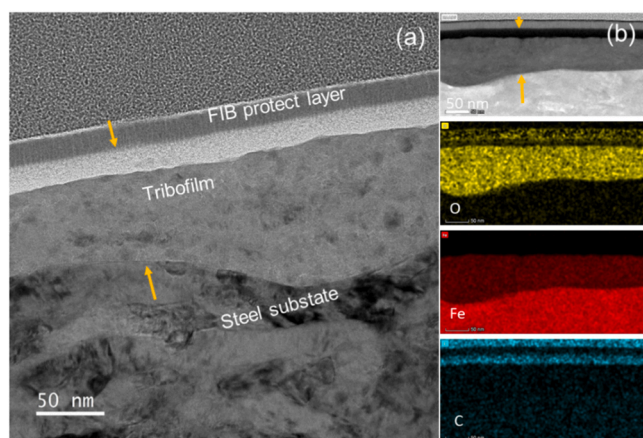


Fig. 9. (a) TEM and (b) HAADF with EDX images of tribofilm with PAO base oil.

in Fig. 10, reveals that the film primarily consists of amorphous iron oxide and carbon. Although boron could not be detected using EDX due to its low energy, its presence within the tribofilm was confirmed through Electron Energy Loss Spectroscopy (Fig. 10c). The sharp peak at 195 eV, corresponding to transitions to non-bonding π^* (P_z) orbitals, and the broad feature around 203 eV, attributed to σ^* orbitals, together suggest the presence of B₂O₃ [50] within the tribofilm. Combined with the boron oxide signal observed in the negative SIMS results, it is suggested that BN nanoparticles do not form the tribofilm on the steel substrate directly. Instead, a tribochemical reaction occurs between the BN and the steel substrate due to the high pressure and flash temperature generated by the contact of rough peaks [23,51]. This reaction promotes the formation of compounds such as boron oxides and iron oxides in the contact region, which subsequently accumulate to form the tribofilm.

In the tribofilm structure formed with TiO₂ nanoparticles (Fig. 11), a thin carbon layer with a few nanometres thick is present on the surface, while titanium is uniformly distributed throughout the bulk of the tribofilm (Fig. 11b). This uniform distribution indicates that the incorporation of TiO₂ nanoparticles leads to the even integration of titanium into the tribofilm, which primarily consists of iron oxide and carbon when using pure PAO base oil. The homogeneous presence of titanium suggests that TiO₂ influences the tribofilm structural and compositional uniformity, effectively doping it with titanium. Given the uniform distribution of titanium within the tribofilm, it is likely that it is not merely physically incorporated but participates in chemical interactions during the tribological process. The dissociated short-chain dehydrogenated hydrocarbons from PAO base oil may react with oxygen from environment to form carboxyl groups. These carboxyl groups could chelate with titanium and iron, generating metal-organic compounds [52] that contribute to the formation of the robust tribofilm. This finding demonstrates the potential to fabricate thin films through the tribological process while simultaneously doping them with other beneficial elements using nanoparticles.

The five different nanoparticles selected in this work have all been reported to form the tribofilm through tribochemical reactions in the previous research. However, in this study, only TiO₂ and BN were detected in the fabricated tribofilm after the tests. Given that the present study was performed without variation of sizes for each type of nanoparticles (Table 1), it is not possible to confirm the role of nanoparticle size as an independent parameter to affect the tribofilms formation. Nevertheless, a potential explanation for this observation relates to the particle size and surface roughness. It is generally accepted that particles smaller than the surface roughness are more likely to remain in the contact zone during loading and shearing [53]. The roughness of the steel substrate is 57.8 ± 1.02 nm, while TiO₂ has the smallest particle size of less than 25 nm compared to the other nanoparticles. Due to its smaller initial size relative to the average steel substrate surface roughness, the TiO₂ nanoparticle can enter the contact area [54] and

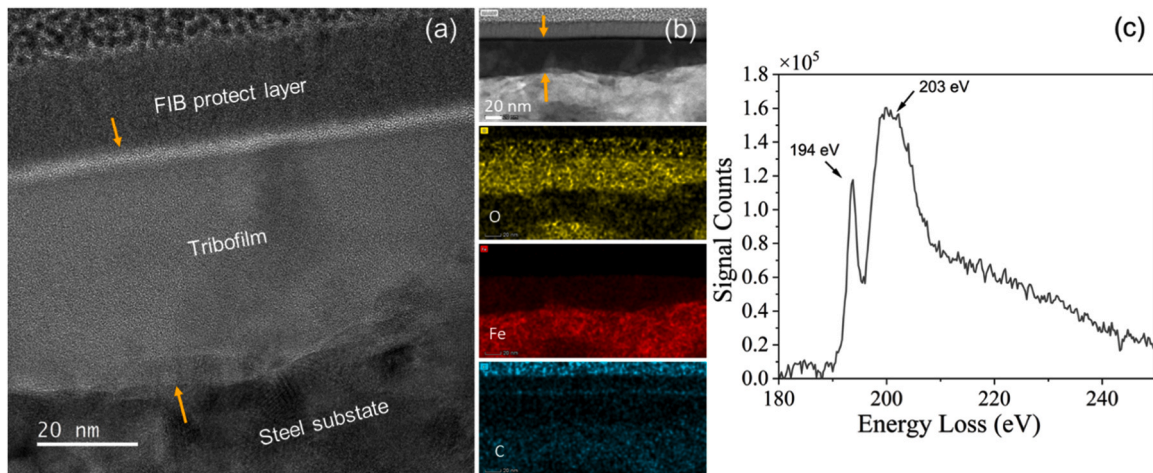


Fig. 10. (a)TEM of tribofilm with BN nanoparticle, (b)HAADF with EDX images and (c)EELS spectrum of tribofilm area.

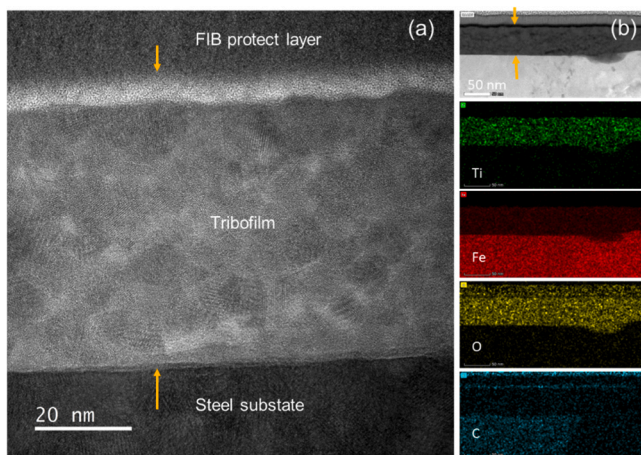


Fig. 11. (a)TEM and (b)HAADF with EDX images of tribofilm with TiO_2 nanoparticle.

react with the substrate to form the tribofilm. The Al_2O_3 nanoparticles used in this study are of a similar size to those reported in the literature to form tribofilms [36]. That study also concluded that Al_2O_3 nanoparticles exhibit greater reactivity with the polyphosphate matrix present in commercial engine oils. The absence of polyphosphate compounds in the PAO base oil used in this work may have contributed to the lack of Al_2O_3 incorporation into the fabricated tribofilm. Furthermore, previous research suggests that tribo-sintering of CuO nanoparticles is more likely to occur with ultra-fine particles, typically only a few nanometers in size [33]. Therefore, except the influence of particle size and surface roughness, the successful fabrication of CuO -based tribofilms via tribo-sintering may require nanoparticles with extremely fine dimensions

In the absence of dispersants and other additives, WS_2 nanoparticles with a size larger than the surface roughness were unable to be used to fabricate the tribofilm. This finding supports the conclusion that nanoparticles must be smaller than the surface asperities to be effective [55]. For BN, despite its particle size being larger than the surface roughness. The aggregated large-sized nanoparticles may exhibit poor flowability, which could allow them to enter the contact area under contact extrusion [56]. Furthermore, under increased contact stress, exfoliation of one or several BN layers is highly possible [57], further increasing the likelihood of these particles entering the contact area and undergoing tribochemical reactions. Therefore, despite having the largest size among the nanoparticles investigated in this work, some BN

nanoparticles can still enter the contact area and contribute to the formation of the tribofilm. A systematic variation of nanoparticle sizes in future studies will clarify the role of nanoparticle size in the formation of tribofilms as an independent parameter.

4. Conclusions

Five types of nanoparticles, along with PAO base oil, were selected to investigate their performance in fabricating thin films during the tribology process:

- A methodology utilising Conductive Atomic Force Microscopy (CAFM) has been developed that could accurately characterise the distribution and thickness of tribofilms.
- For PAO base oil, a tribofilm composed of carbon and iron oxides can be fabricated on the steel surface. The iron oxide wear debris increased the dissociation rate of C–C and C–H bonds in linear olefins and facilitated the formation of the two-layer tribofilm structure.
- BN and TiO_2 can be incorporated into the tribofilm through tribochemical reactions, altering the composition of the fabricated thin film compared with PAO base oil. With the particle size less than the average surface roughness, TiO_2 could enter the contact area and chelate with the carboxyl groups and iron to generate metal-organic compounds that form a robust tribofilm. Large size BN nanoparticles with low flowability could be extruded into the contact area and react to form an unevenly distributed tribofilm.
- The addition of WS_2 , Al_2O_3 , and CuO nanoparticles influences the thickness and distribution of the resulting two-layer tribofilm from PAO base oil but does not alter its chemical composition. We propose that with particle sizes equal to or above the surface roughness level, it becomes difficult for these nanoparticles to enter the contact area and react to form the tribofilms; this hypothesis will be verified with varying nanoparticle sizes in future study.

The incorporation of nanoparticles to generate tribofilms opens new pathways for the fabrication of thin films. With the newly developed CAFM methodology, the morphology of the fabricated thin film with nanoparticles can be well characterised. Compared with conventional approach to characterise the tribofilm thickness over a cross-section, e. g., TEM and EDX, this new methodology was able to provide 3-dimensional surface profiles of tribofilms, revealing a general distribution of tribofilms on the surface. Future work can leverage the unique characteristics of nanoparticles, such as their electrical, thermal, and optical attributes, to develop more versatile tribofilms that could be used in applications not just reducing friction and wear. These films could find

broader applications, including in microelectronics, energy storage, and biosensors, where precise control of film properties like conductivity and photosensitivity is needed.

CRedit authorship contribution statement

Yuyang Yuan: Writing – review & editing, Writing – original draft, Methodology, Data curation, Conceptualization. Chun Wang: Writing – review & editing, Supervision, Methodology, Conceptualization. Seunghwan Lee: Writing – review & editing, Methodology. Mark C.T. Wilson: Supervision. Ardian Morina: Writing – review & editing, Supervision, Project administration, Funding acquisition, Conceptualization.

Declaration of Competing Interest

The authors declare that they have no known competing financial interests or personal relationships that could have appeared to influence the work reported in this paper.

Acknowledgements

This work received funding from the EPSRC TRibology as an ENabling Technology (TRENT) grant EP/S030476/1. TEM/EDX data collection took place at Leeds Electron Microscopy and Spectroscopy Centre and the authors would like to thank Stuart Micklethwaite and Dr Zabeada Aslam for their technical support and discussions.

Appendix A. Supporting information

Supplementary data associated with this article can be found in the online version at [doi:10.1016/j.triboint.2025.110805](https://doi.org/10.1016/j.triboint.2025.110805).

Data availability

Data will be made available on request.

References

- Chen Y, Renner P, Liang H. A review of current understanding in tribochemical reactions involving lubricant additives. *Friction* 2022;11(4):489–512.
- Georges JM, et al. Mechanism of boundary lubrication with zinc dithiophosphate. *Wear* 1979;53(1):9–34.
- Dorgham A, et al. In situ synchrotron XAS study of the decomposition kinetics of ZDDP triboactive interfaces. *RSC Adv* 2018;8(59):34168–81.
- Gosvami NN, et al. Tribology. Mechanisms of antiwear tribofilm growth revealed in situ by single-asperity sliding contacts. *Science* 2015;348(6230):102–6.
- Zhang J, Spikes H. On the mechanism of ZDDP antiwear film formation. *Tribology Lett* 2016;63(2).
- Fang L, et al. What stress components drive mechanochemistry? A study of ZDDP tribofilm formation. *Faraday Discuss* 2023;241(0):394–412.
- Dorgham A, et al. Single-asperity study of the reaction kinetics of P-based triboactive films. *Tribol Int* 2019;133:288–96.
- Phan HP, et al. Robust free-standing nano-thin SiC membranes enable direct photolithography for MEMS sensing applications. *Adv Eng Mater* 2017;20(1):1700858.
- Chou SY, Keimel C, Gu J. Ultrafast and direct imprint of nanostructures in silicon. *Nature* 2002;417(6891):835–7.
- Deng J, et al. Electron beam lithography on uneven resist for uniform Bragg gratings in GaSb based distributed-feedback lasers. *Microelectron Eng* 2018;195:32–5.
- Ryu Cho YK, et al. Sub-10 nanometer feature size in silicon using thermal scanning probe lithography. *ACS Nano* 2017;11(12):11890–7.
- Wang Y, et al. AFM tip hammering nanolithography. *Small* 2009;5(4):477–83.
- Dorgham A, et al. 3D tribo-nanoprinting using triboactive materials. *Nanotechnology* 2019;30(9):095302.
- Khare HS, et al. Nanotribological printing: a nanoscale additive manufacturing method. *Nano Lett* 2018;18(11):6756–63.
- Khare HS, et al. Nanoscale generation of robust solid films from liquid-dispersed nanoparticles via in situ atomic force microscopy: growth kinetics and nanomechanical properties. *ACS Appl Mater Interfaces* 2018;10(46):40335–47.
- Senthil Kumar K, Chen PY, Ren H. A review of printable flexible and stretchable tactile sensors. *Res (Wash D C)* 2019;2019:3018568.
- Duston S, et al. Tribological manufacturing of ZDDP tribofilms functionalised by graphene nanoplatelets. *J Phys: Mater* 2024;7(4).
- Farhanah Azman N, et al. Tribological performance and mechanism of graphite, hBN and MoS₂ as nano-additives in palm kernel oil-based lubricants: a comparative study. *J Mol Liq* 2024;410.
- Balik M, Bulut V, Erdogan IY. Optical, structural and phase transition properties of Cu₂O, CuO and Cu₂O/CuO: their photoelectrochemical sensor applications. *Int J Hydrog Energy* 2019;44(34):18744–55.
- Ali MKA, et al. Minimizing of the boundary friction coefficient in automotive engines using Al₂O₃ and TiO₂ nanoparticles. *J Nanopart Res* 2016;18(12).
- Ratoi M, et al. Mechanism of action of WS₂ lubricant nanoadditives in high-pressure contacts. *Tribology Lett* 2013;52(1):81–91.
- Lineira del Río JM, et al. Tribological enhancement of potential electric vehicle lubricants using coated TiO₂ nanoparticles as additives. *J Mol Liq* 2023;371.
- Wen G, et al. Effect of mixing procedure of oleic acid and BN nanoparticles as additives on lubricant performance of PAOS. *Tribol Int* 2022;175.
- Greco A, et al. Friction and wear behaviour of boron based surface treatment and nano-particle lubricant additives for wind turbine gearbox applications. *Wear* 2011;271(9-10):1754–60.
- Thrush SJ, et al. Growth and morphology of thermally assisted sinterable zirconia nanoparticle tribofilm. *Tribol Int* 2022;175.
- Thrush SJ, et al. Study of pressure dependence on sinterable zirconia nanoparticle tribofilm growth. *Tribol Int* 2021;154.
- Xu W, et al. 3D printing-enabled nanoparticle alignment: a review of mechanisms and applications. *Small* 2021;17(45):e2100817.
- Yi C, et al. Polymer-guided assembly of inorganic nanoparticles. *Chem Soc Rev* 2020;49(2):465–508.
- Han T, et al. Fully 2D materials-based resistive switching circuits for advanced data encryption. *Adv Funct Mater* 2024;34(41).
- Wei X-F, et al. Obtaining ultra-high throwing power in Cu electroplating of flexible printed circuit by fast consumption of a suppressor. *J Solid State Electrochem* 2021;26(1):171–81.
- Sharma S, et al. Temperature dependent photoluminescence from WS₂ nanostructures. *J Mater Sci: Mater Electron* 2018;29(23):20064–70.
- Hu H, et al. In-plane aligned assemblies of 1D-nanoobjects: recent approaches and applications. *Chem Soc Rev* 2020;49(2):509–53.
- Alves SM, et al. Nanolubricants developed from tiny CuO nanoparticles. *Tribol Int* 2016;100:263–71.
- Dassenoy F, et al. Performance and lubrication mechanism of new TiO₂ nanoparticle-based high-performance lubricant additives. *Tribol Trans* 2020;64(2):325–40.
- Thottackkad MV, Perikinalil RK, Kumarapillai PN. Experimental evaluation on the tribological properties of coconut oil by the addition of CuO nanoparticles. *Int J Precis Eng Manuf* 2012;13(1):111–6.
- Ma F, et al. Evaluation of tribological performance of oxide nanoparticles in fully formulated engine oil and possible interacting mechanism at sliding contacts. *Surf Interfaces* 2021;24.
- Peña-Parás L, et al. Effect of CuO and Al₂O₃ nanoparticle additives on the tribological behavior of fully formulated oils. *Wear* 2015;332-333:1256–61.
- Szabó AI, et al. Experimental wear analysis of nano-sized titania particles as additives in automotive lubricants. *Micro* 2023;3(3):715–27.
- Erdemir A, et al. Carbon-based tribofilms from lubricating oils. *Nature* 2016;536(7614):67–71.
- Feng W, et al. On the mechanical and tribological performances of the tribofilm formed by zinc dialkyl dithiophosphate. *J Ind Eng Chem* 2023;122:152–60.
- Huynh KK, et al. Tribo-induced catalytically active oxide surfaces enabling the formation of the durable and high-performance carbon-based tribofilms. *Tribol Int* 2023;184.
- Hernández Battez A, et al. CuO, ZrO₂ and ZnO nanoparticles as antiwear additive in oil lubricants. *Wear* 2008;265(3-4):422–8.
- Wu X, et al. Adaptive TiN-Cu/PAO composite lubrication system: the tribocatalysis-induced PAO6 transferring to amorphous carbon. *Tribol Int* 2024;196.
- Lassoued A, et al. Control of the shape and size of iron oxide (α-Fe₂O₃) nanoparticles synthesized through the chemical precipitation method. *Results Phys* 2017;7:3007–15.
- Sparavigna AC. Raman spectroscopy of the iron oxides in the form of minerals. *Part Nanopart* 2023.
- Kaluzny J, et al. The indirect tribological role of carbon nanotubes stimulating zinc dithiophosphate anti-wear film formation. *Nanomater (Basel)* 2020;10(7).
- Hruska B, et al. Thermodynamic model and Raman spectra of BaO-B₂O₃ glasses. *Vib Spectrosc* 2019;105.
- Huynh KK, et al. Tribocatalysis induced carbon-based tribofilms—an emerging tribological approach for sustainable lubrications. *Lubricants* 2023;11(8).
- Ta TD, Kiet Tieu A, Tran BH. Influences of iron and iron oxides on ultra-thin carbon-based tribofilm lubrication. *Tribol Int* 2022;173.
- Mountjoy G, Corrias A, Gaskell PH. An electron energy loss spectroscopy study of Ni₆₀B₄₀ alloys prepared by chemical reduction and melt spinning. *J Non-Cryst Solids* 1995;192-193:616–9.
- Yang G, et al. Preparation of triazine derivatives and evaluation of their tribological properties as lubricant additives in poly-alpha olefin. *Tribol Int* 2013;62:163–70.
- Zhang X, et al. Synergism of TiO₂ and Ni on the growth of a double-layered tribofilm: new strategy for ZDDP replacement. *ACS Sustain Chem Eng* 2024;12(15):5831–41.

- [53] Uflyand IE, Zhinzhiro VA, Burlakova VE. Metal-containing nanomaterials as lubricant additives: State-of-the-art and future development. *Friction* 2019;7(2): 93–116.
- [54] Peña-Parás L, et al. Effects of substrate surface roughness and nano/micro particle additive size on friction and wear in lubricated sliding. *Tribol Int* 2018;119:88–98.
- [55] Rapoport L, et al. Behavior of fullerene-like WS₂ nanoparticles under severe contact conditions. *Wear* 2005;259(1-6):703–7.
- [56] Wu H, Wang L, Dong G. Origin of the tribofilm from MoS₂ nanoparticle oil additives: Dependence of oil film thickness on particle aggregation in rolling point contact. *Friction* 2020;9(6):1436–49.
- [57] Bondarev AV, et al. Mechanisms of friction and wear reduction by h-BN nanosheet and spherical W nanoparticle additives to base oil: Experimental study and molecular dynamics simulation. *Tribol Int* 2020;151.